Journal of Alloys and Compounds 500 (2010) 241–246

Contents lists available at ScienceDirect

Journal of Alloys and Compounds

journal homepage: www.elsevier.com/locate/jallcom

XRD and electrochemical investigation of particle size effects in platinum-cobalt cathode electrocatalysts for oxygen reduction

I.N. Leontyev[a,b,*], V.E. Guterman[b], E.B. Pakhomova[b], P.E. Timoshenko[b], A.V.Guterman[b], I.N. Zakharchenko[b], G.P. Petin[b], B. Dkhil[a]

[a] Laboratoire Structures, Proprietes et Modelisation des Solides, Ecole Centrale Paris, CNRS-UMR8580 Grande Voie des Vignes, F-92295, Chatenay-Malabry Cedex, France
[b] Southern Federal University, 5 Zorge St., Rostov-on-Don, 344090 Russia

ARTICLE INFO

Article history:
Received 9 October 2009
Received in revised form 28 March 2010
Accepted 1 April 2010
Available online 13 April 2010

Keywords:
Platinum alloy
Electrocatalysis
Grain size distribution
Oxygen reduction reaction (ORR)
X-ray diffraction (XRD)

ABSTRACT

Pt-Co/C electrocatalysts with Pt loadings close to 30 wt.% prepared by the impregnation method in water–ethylene glycol solutions were investigated by X-ray diffraction and correlated with electrochemical measurements. We show that composition of the binary solvent controls the average particle size and its distribution. The unit cell parameter of the Pt_3Co alloy decreases nonlinearly with decreasing particle size. The ORR activity of the prepared Pt-Co/C catalysts in H_2SO_4 solution enhances with decreasing particle size and unit cell parameter as well as with narrowing of the particle size distribution. Corrosion treatment of the synthesized Pt-Co/C materials brings about an increase of ca. 1 nm in the average grain size accompanied by broadening of the grain size distribution and a decrease in the Co content. All of the synthesized Pt-Co/C materials show higher ORR activities compared with commercial Pt/C electrocatalysts.

1. Introduction

Proton-exchange membrane fuel cells (PEMFC) have received considerable attention as promising devices for portable and transport applications due to their high energy density, relatively low operating temperature and minimal corrosion problems. Yet, the commercial viability of the PEMFC's has been hindered by a number of factors including the high cost, insufficient stability against degradation, and agglomeration of the Pt nanoparticles. The latter two are especially intrinsic to the oxygen electrode. They reduce the catalyst's effective surface and hence the activity. A search for more active, cost-effective, and corrosion stable electrocatalysts for the oxygen reduction reaction is therefore a priority in the fuel cell catalysis area. The most popular strategy toward more active, stable and more tolerant to the presence of poisons electrocatalysts has been alloying pure Pt with metals (Me), such as Fe [1], Ni [2,3], Co [4], Cu [5], Ru [6,7], etc. It has been suggested [8–13] that the activating effect of the alloying elements for the ORR could be associated with (i) modified composition of the surface oxides and improved corrosion resistance of the alloy; (ii) the formation of a new electronic structure of the metal; (iii) shortening of the Pt–Pt distance which favours adsorption of oxygen molecules; (iv) the formation of a thin Pt shell at the surface of the nanoparticles due to selective dissolution of a second alloying element, and (v) some other weaker effects. One or another mechanism may prevail depending on a specific alloy composition and conditions of the reaction process. The positive effect of the second alloying component on the catalyst's aggregation stability seems to result from strengthening of the nanoparticle to carbon carrier adhesion and/or improved corrosion resistance of the carbon surface regions adjacent to the metal nanoparticles [8,14]. Unfortunately, the second component in such alloys is not as stable as Pt, and the alloy composition may alter owing to corrosion during operation of an electrocatalyst [10,12]. The corrosion effect on the composition and structure of a Pt-Me/C catalysts as well as the dependence of the catalyst's stability on its original composition and structure are therefore items of great importance.

In reality, carbon carries the catalyst nanoparticles of different size, and its metal coverage itself is variable and not always uniform [8,11,15,16]. Optimum size range of the metal nanoparticles is altogether uncertain and is apparently dependent on a particular electrochemical system, conditions of the reaction process, and the alloy composition. The above considerations demonstrate that control over composition and size of the metal alloy nanoparticles is a real challenge both in science and technology.

This work was undertaken in order to (i) study the influence of the water–ethylene glycol solvent composition on structural and micro structural parameters of the Pt_3Co/C materials prepared by wet synthesis; (ii) investigate the particle size effect in the synthe-

* Corresponding author at: Southern Federal University, 5 Zorge, Rostov-on-Don 344090, Russia.
E-mail address: i.leontiev@rambler.ru (I.N. Leontyev).

0925-8388/$ – see front matter © 2010 Elsevier B.V. All rights reserved.
doi:10.1016/j.jallcom.2010.04.018

Table 1
Characteristics of Pt-Co/C electrocatalysts prepared by borohydride synthesis.

Sample	PC1	PC3	PC5
Water concentration in solvent (vol.%)	17	50	83
Theoretical composition	Pt_3Co/C	Pt_3Co/C	Pt_3Co/C
Metal loading (wt.%)	24	28	30

sized Pt_3Co/C electrocatalysts by means of XRD, and (iii) estimate the ORR activity and corrosion stability of the synthesized materials in H_2SO_4.

2. Experimental

2.1. Preparation of the electrocatalysts

Carbon-supported Pt–Co electrocatalysts with nominal Pt:Co atomic ratio of 3:1 were prepared by a low temperature method using sodium borohydride as a reducing agent [17]. A high surface area carbon (Timrex HSAG-300) was impregnated with solutions of chloroplatinic acid ($H_2PtCl_6{\cdot}6H_2O$) and cobalt nitrate ($Co(NO_3)_2{\cdot}6H_2O$). The metals were then reduced at room temperature by a sodium borohydride solution which was added to the carbon dispersion at pH = 10 under sonication. The water/ethylene glycol mixture was used as a solvent. Water and the nonaqueous component of the solvent were taken in ratios of 1:5, 1:1, and 5:1 for samples denoted as PC1, PC3, and PC5, respectively. The resulting material represented 24–30 wt.% metal on the carbon support (see Table 1). All prepared samples were treated in 1 M H_2SO_4 at 100 °C for 1 h in order to estimate of the corrosion and aggregate stabilities. The treated samples were denoted as PC2, PC4, and PC6, respectively.

Metal loadings in the Pt-Co/C materials were determined by differential thermal analysis using a Diamond TG/DTA derivatograph (PerkinElmer). The Pt:Co atomic ratios in the synthesized catalysts were ascertained by means of an energy dispersive X-ray spectrometry system DX-95 (EDAX, Inc.).

2.2. Electrochemical measurements

To test the catalytic activity of the prepared Pt_3Co/C materials, the rotating disk electrode (RDE) method was used. The glass-carbon electrode's butt-end was soaked with a drop of the catalyst's alcohol suspension containing a small amount of polyvinylidenefluoride. The RDE was rotated at 1000 rpm and stabilized at 0.72 V with an IPC-Pro potentiostat during the current measurements. The electrolyte was a 1 M H_2SO_4 solution saturated with oxygen (p = 1 atm). The potentials cited in this work are all referred to that of the reversible hydrogen electrode.

2.3. X-ray diffraction (XRD)

Powder diffraction patterns were recorded at the Swiss–Norwegian Beam Lines (SNBL) at the ESRF (λ = 0.72287 Å) using a MAR345 image-plate detector. The wavelength, sample to detector distance (150 mm) and resolution of the setup were calibrated with LaB_6 powder (NIST) [18]. The samples were loaded into glass capillaries (Hilgenberg GmbH) having a diameter of 0.3 mm and a wall thickness of 0.01 mm. The data were processed with the Fit2D software [19].

2.4. XRD data processing

The peak shapes were described using the pseudo-Voigt function [20]. The X-ray reflections were fitted using the Winplotr from the FullProf software [21]. The goodness-of-fit is illustrated in Fig. 1. It should be noted that our fittings were made

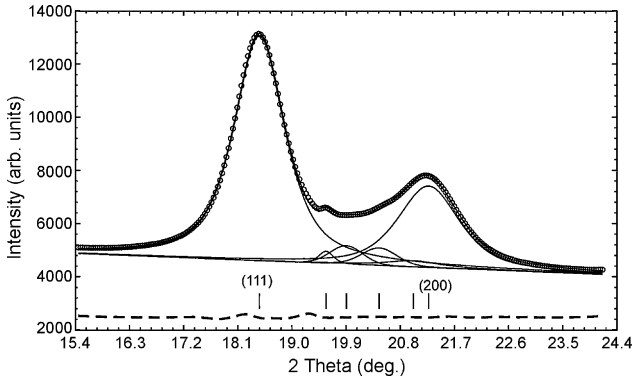

Fig. 1. Goodness-of-fit for the observed (1 1 1) and (2 0 0) reflections (open circles), fitted data (solid curve) and the difference (dashed curve).

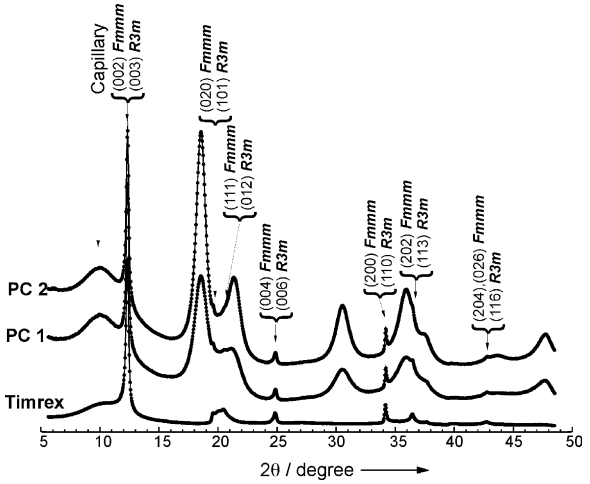

Fig. 2. XRD patterns of carbon-supported Pt-Co/C catalysts (samples PC1, PC2) and of the carbon support itself (Timrex HSAG-300).

with allowance for the reflections from the carbon support. Ignorance of that contribution could lead to erroneous determinations of the Bragg angle 2θ and the full width at half maximum (FWHM), hence underestimation of the particle size (our estimated error is about 0.2 nm for particle sizes close to 3 nm). XRD pattern of the carbon support (Timrex HSAG-300) representing a mixture of the rhombohedral *R3m* (a = 3.6420 Å, α = 39°30) and orthorhombic *Fmmm* (a = 2.456 Å, b = 4.254 Å, c = 6.696 Å) graphite phases is shown in Fig. 2.

The average grain size was determined by three separate techniques. The first was the so-called "double-Voight", method [22]. The main relations in this method are

$$\beta_L = \beta_{LS} + \beta_{LD}\frac{s^2}{s_0^2}, \quad \beta_G^2 = \beta_{GS}^2 + \beta_{GS}^2\frac{s^2}{s_0^2},$$

where $s = 2\sin\theta/\lambda = 1/d$, β_L, β_G are the integral breadths of Lorentz (L) and Gauss (G) functions, and β_{LS}, β_{GS}, β_{LD}, β_{GD} are the integral breadths of Lorentz and Gauss functions, corresponding to the size (S) or strain (D) broadenings.

For the Voigt size-broadened profile, the size coefficient is given by the Fourier transform $A_S(L) = \exp(-2L\beta_{LS} - \pi L^2\beta_{GS}^2)$, where $L = n|a_3|$ is the length of columns of cells along the a_3 direction normal to the diffracting planes. The second derivative of the size coefficient, $\frac{d^2A(L)}{dL^2} = [(2\pi L\beta_{GS}^2 + 2\beta_{LS})^2 - 2\pi\beta_{GS}^2]A_S(L)$, defines the size distribution function $p_V(L) \propto L(d^2A(L)/dL^2)$. The respective mean values for the volume-weighted grain size are given as

$$\bar{D}_V = \frac{\int_0^\infty Lp_V(L)dL}{\int_0^\infty p_V(L)dL} = \frac{\exp(k_S^2)}{\beta_{GS}}erfc(k_S),$$

where $k_S = \beta_{LS}/(\sqrt{\pi}\beta_{GS})$.

Determination of the volume-weighted grain size was carried out by means of the Balzars program BREADTH [23].

The second method is based on the assumption that the grain size distribution (GSD) obeys a Gamma function

$$\mathrm{GSD}(D : D_0, m) = \frac{D_0^{-m-1}}{(m+1)}D^m e^{-D/D_0},$$

where $D_0 = \sigma^2/\bar{D}$, $m = (\bar{D}/\sigma)^2 - 1$, which is very close to the conventional lognormal distribution. A detailed description and justification of this method, called the FW$\frac{1}{5}$/$\frac{4}{5}$M one, can be found in Ref. [24]. The average grain size $\bar{D}$ and its dispersion σ are derived from the expressions

$$\bar{D} = \frac{2BC}{\mathrm{FW}\frac{4}{5}\mathrm{M}}, \quad \sigma = \frac{2B\sqrt{C}}{\mathrm{FW}\frac{4}{5}\mathrm{M}}.$$

The coefficients B and C were found from the expressions

$$A = \mathrm{arcctg}(277069 - 105723\mathrm{FW}\frac{1}{5}/\frac{4}{5}\mathrm{M}),$$

$$B = 0.001555 + 0.00884 \times \mathrm{ctg}(0.002237 - 2101 \times A),$$

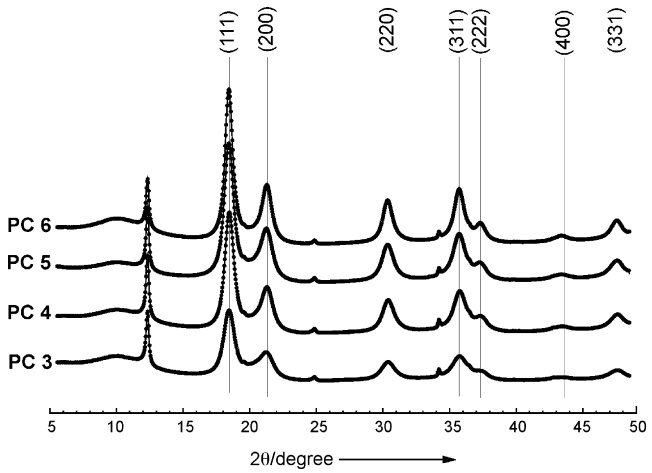

Fig. 3. XRD patterns of carbon-supported Pt-Co/C catalysts (samples PC3–PC6).

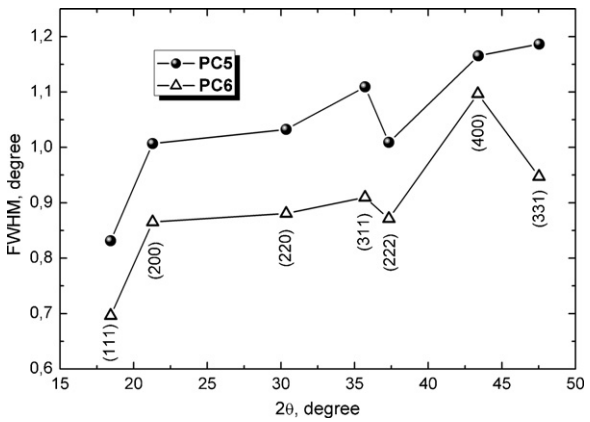

Fig. 4. FWHM values vs. 2θ for as-prepared (PC5) and treated (PC6) samples of Pt-Co/C catalyst.

$$C = -0.6515 - 463695 \times A,$$

where $FW\frac{1}{5}M$ and $FW\frac{4}{5}M$ are the full widths at 1/5 and 4/5 of the peak maximum, respectively. As was shown in Ref. [25], the grain size distribution determined by this method for the strain-free samples is in good agreement with that found from the SEM analysis. For determination of the GSD by this method we have developed the L&TGSD program (http://www.nanotechnology.sfedu.ru/index.php?page=rus.faculty.projects).

The third way applied here for determination of the average grain size is based on the well-known Scherrer equation $\bar{D} = K\lambda/(H_{PV}\cos\theta)$ [26], where λ is the wavelength; $\bar{D}$ is the volume averaged grain size; θ is the Bragg angle, and $K = 0.89$ is the Scherrer constant in our X-ray geometry.

The fitting results for the (1 1 1) peak were employed for estimation of the average grain size and the GSD parameters using the Scherrer equation and the $FW\frac{1}{5}/\frac{4}{5}M$ method. The (1 1 1) and (2 2 2) peaks were used for the "double-Voight", method. Corrections for the instrumental broadening were made according to a conventional procedure described, e.g., in Ref. [27].

Transmission electron microscopy (TEM) analysis was performed using a Tecnai 12 microscope (Philips, Netherlands) operated at an accelerating voltage of 100 kV. To prepare samples for the analysis, the catalyst powders were ultrasonically suspended in ethanol, then applied onto a copper grid and dried in air. Scanning electron microscopy (SEM) images were taken with a ZEISS Supra 25 unit operated at 20 kV.

3. Results and discussion

The XRD patterns of all our Pt-Co/C samples, both as-prepared and treated in boiling H_2SO_4, are presented in Figs. 2 and 3. One can see the pronounced peaks characteristic of a Pt–Co alloy with the fcc structure. No obvious peaks indicating the presence of free Co or its oxides are present (see Figs. 2 and 3).

Examination of the FWHM values for all the samples revealed the occurrence of anisotropic line broadening. Fig. 4 shows the FWHM values at different Bragg angles for the as-prepared (PC5) and treated (PC6) samples where the anisotropy is most pronounced. The (1 1 1) reflection has consistently lower FWHM's compared to the other reflections, and the anisotropy increases with increasing grain size. In general, the anisotropic line broadening may be attributed to the three factors: the presence of stacking faults, the presence of dislocations, and nonequivalence of the grain sizes along different crystallographic directions. In our case, it is due to the grain size anisotropy. The presence of stacking faults would provoke a reduced coherent scattering region along the ⟨1 1 1⟩ direction (as compared to those along other directions) hence a higher FWHM value. The occurrence of dislocations is hardly probable since it was shown [28,29] that the metal particles became dislocation-free below a certain critical size. For instance, dislocation-free particles of iron and nickel have diameters of 23 and 140 nm, respectively [29]. The same is evident from the high-resolution TEM images of the Pt_3Co and $Pt_{69}Ni_{31}$ particles [10,14].

Values of the average grain size along the (1 1 1) direction, $\bar{D}_{111}$ estimated using the "double-Voight", the $FW\frac{1}{5}/\frac{4}{5}M$, and the Scherrer methods are listed in Table 2 for the synthesized Pt-Co/C samples. Although individual $\bar{D}_{111}$ values may vary from sample to sample, they show almost identical dependences on the solvent composition both prior and subsequent to the treatment. As follows from Table 2, despite a discrepancy in the grain size values for each individual sample, all the three techniques yield nearly identical variation of the dimension of the as-prepared Pt-Co nanoparticles as a function of ethylene glycol concentration in the solvent, and very similar changes subsequent to the treatment. Thus, the average grain size increases in the sequence PC1 < PC3 < PC5 as the concentration of the organic component is lowered and the treatment in H_2SO_4 brings about an additional increase of ca. 0.8–1 nm.

To compare the XRD and microscopy results on the average grain size, the as-prepared sample PC1 was chosen. The SEM image of Fig. 5a shows that the catalyst particles are distributed uniformly over the carbon support in form of individual grains with little or no aggregation. According to the TEM data (Fig. 5b) the average grain size is 3.6 nm which is close to the XRD result given in Table 2.

Table 2
Average particle size, unit cell parameter *a*, Pt–Pt distance, and alloy composition of the nanostructured Pt-Co/C electrocatalysts.

Sample		Average particle size				*a* (Å)	Pt–Pt distance (Å)	EDX composition
		Scherrer D_{111} (nm)	Double Voigt D_{111} (nm)	$FW\frac{1}{5}/\frac{4}{5}M$ D_{111} (nm)	σ (nm)			
PC1	As prepared	2.9	2.5	3.1	1.5	3.881	2.744	$Pt_{58}Co_{42}$
PC3		3.8	3.4	4.0	2.1	3.905	2.761	$Pt_{66}Co_{34}$
PC5		4.6	4.3	4.7	2.6	3.908	2.763	$Pt_{70}Co_{30}$
PC2	Treated	4.0	3.3	4.2	2.2	3.893	2.765	$Pt_{85}Co_{15}$
PC4		4.7	4.4	4.9	2.6	3.908	2.763	$Pt_{86}Co_{14}$
PC6		5.6	5.4	5.7	3.2	3.911	2.752	$Pt_{88}Co_{12}$

Average particle size.

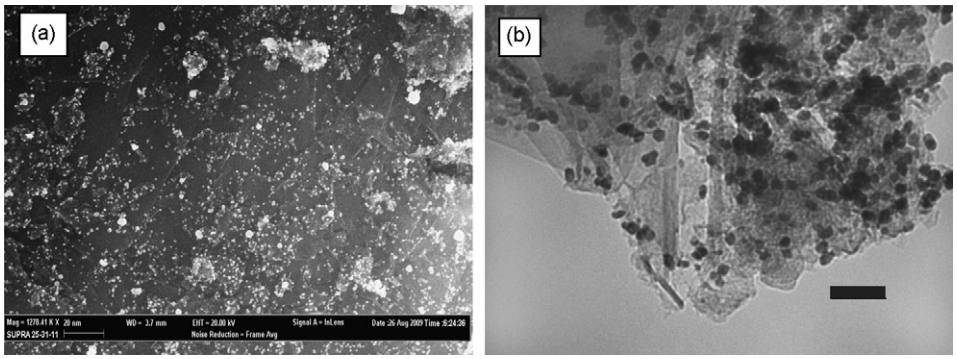

Fig. 5. SEM (a) and TEM (b) images of as-prepared Pt-Co/C catalyst PC1. The scale bar on TEM image is 20 nm.

The minor departure from the value obtained using the Scherrer equation could be due to the formation of an amorphous CoO layer on the grain surfaces. It may as well be attributed to overlapping of the images of different particles situated on the top and bottom surfaces of the carbon support.

Grain size distributions calculated by means of the FW$\frac{1}{5}$/$\frac{4}{5}$M and "double-Voight", methods are presented at Fig. 6 for the as-prepared (PC5) and treated (PC6) samples. The "double Voigt" method, unlike the FW$\frac{1}{5}$/$\frac{4}{5}$M one and the Scherrer equation, takes into account the possible microstrains. Nevertheless the two results agree very closely. It may be concluded that the strain contribution to the observed line broadening is insignificant, and the Scherrer equation and the FW$\frac{1}{5}$/$\frac{4}{5}$M method are both applicable for definition of the average grain size and GSD parameters.

Fig. 7 shows grain size distributions calculated by the FW$\frac{1}{5}$/$\frac{4}{5}$M method for all the three pairs of as-prepared and treated Pt-Co/C samples. The narrowest GSD is found for a 1:5 ratio of water to the nonaqueous component of the solvent. This means that, during synthesis of that material (PC1) the nucleation to growth activation energy ratio E_{nucl}/E_{gr} was the lowest. In such conditions, the nucleation process prevails over particles growth, which corresponds to the instantaneous nucleation model. As the ratio E_{nucl}/E_{gr} increases with water content increasing (samples PC3, PC5), the growth process becomes more favourable, leading to a larger grain size and the GSD broadening (Fig. 6).

Grain size distribution in the synthesized materials becomes broader subsequent to the treatment in H_2SO_4, which is most pronounced in case of the PC1–PC2 pair (Fig. 7). This effect could be due to corrosion of the alloy nanoparticles or carbon at the nanoparticle/support interface. An immediate result would be breakaway of the metal particles from the carbon support and their subsequent agglomeration. Also, in view of a reduced thermodynamic stability of the smaller nanoparticles, one may expect a preferred Pt dissolution of such particles followed by deposition onto the larger ones.

Comparing the unit cell parameters (Table 2) and their dependence on the grain size $\bar{D}_{111}$ (Fig. 8) one may deduce following conclusions: (i) values of a in all the synthesized materials are below that of pure Pt (a_{Pt} = 3.9231 Å [30]). This fact confirms the formation of a Pt-Co solid solution. (ii) A nonlinear a vs. $\bar{D}_{111}$ dependence is

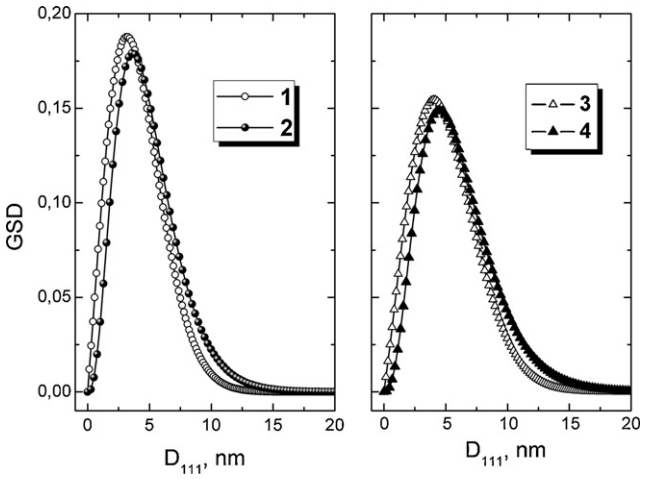

Fig. 6. Comparison of grain size distributions calculated by means of the "double Voigt" (curves 1 and 3) and FW$\frac{1}{5}$/$\frac{4}{5}$M (curves 2 and, 4) methods for as-prepared PC5 (left panel) and treated PC6 (right panel) samples of Pt-Co/C catalyst.

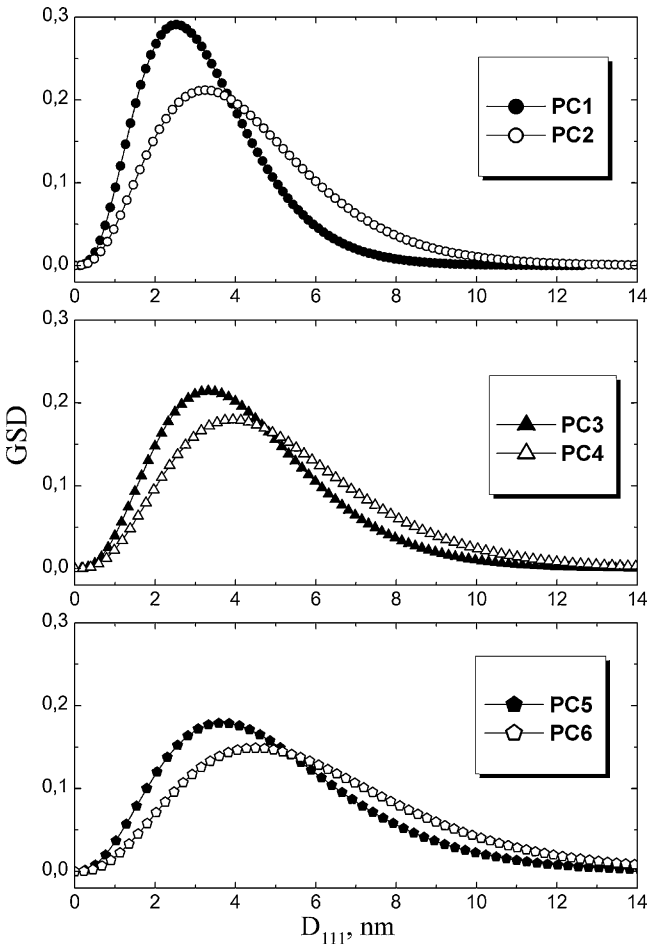

Fig. 7. Grain size distributions as determined by the FW$\frac{1}{5}$/$\frac{4}{5}$M method for as-prepared and treated samples of Pt-Co/C catalysts.

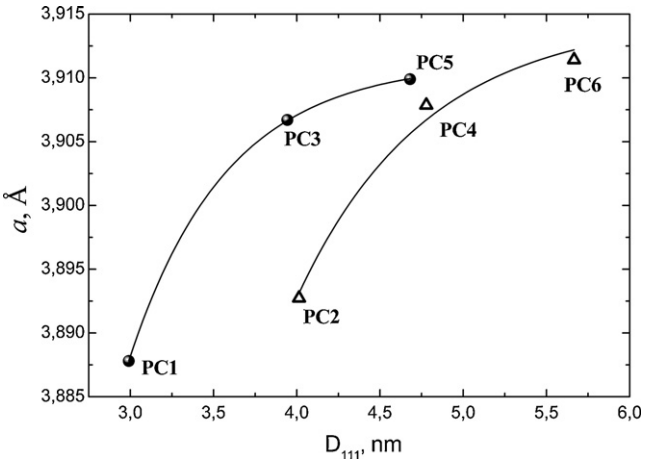

Fig. 8. Unit cell parameter a as a function of particle size D_{111} along the <1 1 1>direction.

observed for the treated samples having practically identical compositions (within the experimental error). This phenomenon could be explained by a size effect which is due to uncompensated interatomic distances and reduced interplanar spacings near the particle surfaces. As a result, the particles become contracted and the unit cell parameter is reduced [31]. The size effect should be more pronounced for smaller nanoparticles where concentration of the surface atoms is essentially higher. A similar effect was observed for nanoparticles of Pd [32] and Ag [33]. The nonlinear a vs. $\bar{D}_{111}$ dependence observed for the as-prepared samples is a consequence of both the aforesaid size effect and different Co concentrations in the crystallites. (iii) Samples denoted as PC4 (the treated PC3) and PC5, although differ essentially in composition, have practically identical unit cell parameters and grain sizes. It therefore seems that a fraction of Co atoms in the starting (as-prepared) samples were not included in the Pt–Co alloy crystallites but were present as an amorphous state. A similar assumption, concerned with dissolution of only "amorphous" Co atoms during a corrosion treatment of Pt-Co/C catalysts was made in Ref. [10].

Cathode chronoamperometric curves for our as-prepared samples demonstrate higher specific currents compared with those measured for the commercial Pt/C electrocatalysts, TEC10V50E (TKK Co., 46% Pt) or E-TEC (40% Pt). The expected and actually observed enhancement of the ORR activity in the PC5 < PC3 < PC1 series (Fig. 9) may be a result of both the enlargement of the metal surface area and an increase in the intrinsic catalytic activity due to

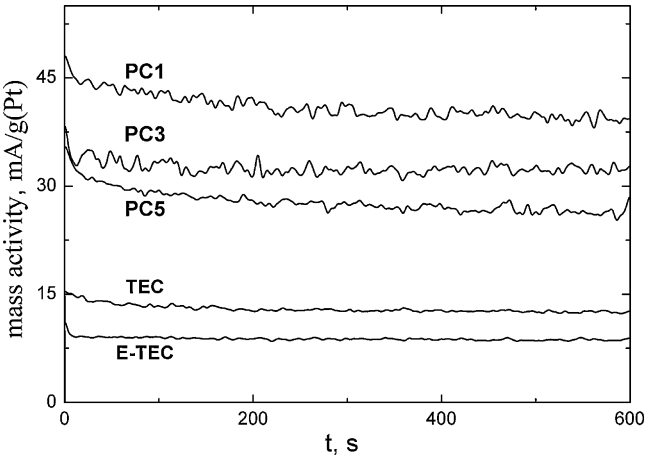

Fig. 9. Room-temperature chronoamperograms of Pt-Co/C catalysts in 1 M H_2SO_4 (O_2 atmosphere, 0.72 V, 1000 rpm).

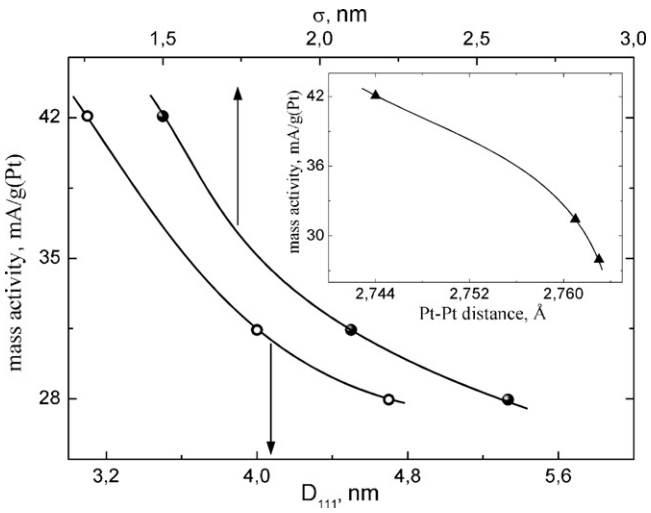

Fig. 10. Mass activity of Pt-Co/C electrocatalysts at 0.72 V (t = 200 s) as function of particle size D_{111} along the <1 1 1>direction, GSD dispersion σ, and Pt–Pt distance (inset).

facilitation of dissociative oxygen adsorption via shortening of the Pt–Pt distances, or the unit cell parameter (Fig. 10).

4. Conclusions

1. The Pt_3Co/C nanoscale materials with average grain sizes of 2.9–4.6 nm and metal loadings of 24–30 wt.% were prepared by wet synthesis using water–ethylene glycol mother solution and $NaBH_4$ as a reducing agent.
2. It was found that the average grain size $\bar{D}_{111}$ of the synthesized materials decreases progressively with increasing concentration of the organic component (ethylene glycol) in the solution.
3. The GSD dispersion σ decreases with decreasing size of the Pt_3Co nanoparticles (higher ethylene glycol concentrations in the solution). The narrowest GSD is observed for a H_2O–ethylene glycol ratio of 1:5.
4. The average grain size increases by 0.8–1 nm, and the grain size distribution becomes broader after treating the Pt_3Co/C samples in hot H_2SO_4 solution.
5. The unit cell parameter dependence on the grain size shows nonlinear behavior both for the as-prepared samples and those treated in hot H_2SO_4.
6. An increase in the anisotropic line broadening with increasing grain size was observed for all of the tested samples. The observed anisotropic line broadening is due to the grain size anisotropy.
7. The mass ORR activity of the prepared Pt_3Co/C catalysts in H_2SO_4 solutions enhances in the order PC5 < PC3 < PC1 (i.e., with decreasing average particle size, unit cell parameter, and GSD dispersion). All of the as-prepared samples show higher catalytic activities compared with commercial Pt/C materials, TEC10V50E (TKK Co., 46% Pt) and E-TEC (40% Pt).

Acknowledgements

The authors wish to thank D. Chernyshov and V. Dmitriev for valuable cooperation and fruitful discussion of the results. The work was supported by The Southern Federal University (internal grant No. 05/6-114) and the Russian Foundation for Basic Research (grant No. 08-08-00869).

References

[1] W. Li, Q. Xin, Y. Yan, Int. J. Hydrogen Energy 35 (2010) 2530–2538.

[2] J. Zhang, H. Yang, J. Fang, S. Zou, Nano Lett. 10 (2) (2010) 638–644.
[3] H. Wu, D. Wexler, G. Wang, J. Alloys Compd. 488 (2009) 195–198.
[4] Q. He, S. Mukerjee, Electrochim. Acta 55 (2010) 1709–1719.
[5] E. Antolini, T. Lopes, E.R. Gonzalez, J. Alloys Compd. 461 (2008) 253.
[6] C. Yang, D. Wang, Xi. Hu, C. Dai, L. Zhang, J. Alloys Compd. 448 (2008) 109–115.
[7] A. Velazquez-Palenzuela, et al., J. Phys. Chem. C 114 (2010) 4399–4407.
[8] D. Thompsett, Handbook of Fuel Cells—Fundamentals, Technology and Applications, Wiley, New York, 2003, pp. 6-1–6-23.
[9] L. Xiong, A.M. Kannan, A. Manthiram, Electrochem. Commun. 4 (2002) 898–903.
[10] N. Travitsky, T. Ripenbein, D. Golodnitsky, Y. Rosenberg, L. Burshtein, E. Peled, J. Power Sources 161 (2006) 782–789.
[11] Hector R. Colon-Mercado, Branko N. Popov, J. Power Sources 155 (2006) 253–263.
[12] E. Antolini, J.R.C. Salgado, E.R. Gonzalez, J. Power Sources 160 (2006) 957–968.
[13] E. Antolini, J.R.C. Salgado, E.R. Gonzalez, J. Power Sources 155 (2006) 161–166.
[14] Xingwen Yu, Siyu Ye, J. Power Sources 172 (2007) 133–144.
[15] V.R. Stamenkovic, B.S. Mun, M. Arenz, et al., Nature 6 (2007) 241–247.
[16] E. Antolini, J.R.C. Salgado, E.R. Gonzalez, J. Electroanal. Chem. 580 (2005) 145–154.
[17] V.E. Guterman, S.V. Belenov, O.V. Dymnikova, T.A. Lastovina, Ya.B. Konstantinova, N.V. Prutsakova, Inorg. Mater. 45 (2009) 498–505.
[18] Standard Reference Materials, vol. 674, National Institute of Standards and Technology, Gaithersburg, MD, USA, 1983.
[19] A.P. Hammersley, S.O. Svensson, M. Hanfland, A.N. Fitch, D. Häusermann, High Pressure Res. 14 (1996) 235–248.
[20] P. Thompson, D.E. Cox, J.B. Hastings, J. Appl. Crystallogr. 20 (1987) 79–83.
[21] T. Roisnel, J. Rodriguez-Carvajal, in: R. Delhez, E.J. Mittenmeijer (Eds.), Proceedings of the Seventh European Powder Diffraction Conference (EPDIC 7), Mater. Sci. Forum (2000) 118–123.
[22] D. Balzar, H. Ledbetter, J. Appl. Crystallogr. 26 (1993) 97–103.
[23] D. Balzar, J. Appl. Crystallogr. 28 (1995) 244–245.
[24] R. Pielaszek, J. Alloys Compd. 382 (2004) 128–132.
[25] A. Vorobiev, D. Chernyshov, G. Gordeev, D. Orlova, J. Appl. Crystallogr. 41 (2008) 831–835.
[26] H.P. Klug, L.E. Alexander, X-ray Diffraction Procedures from Polygrain and Amorphous Materials, Wiley, New York, 1974, p. 275.
[27] S. Vives, E. Gaffet, C. Meunier, Mater. Sci. Eng. A 366 (2004) 229.
[28] V.G. Gryaznov, A.M. Karpelov, A.E. Romanov, Tech. Phys. Lett. 15 (1989) 39–43.
[29] V.G. Gryaznov, I.A. Polonsky, A.E. Romanov, L.I. Trusov, Phys. Rev. B 44 (1991) 42–46.
[30] R.T. Downs, K.L. Bartelmehs, G.V. Gibbs, M.B. Boisen, Am. Min. 78 (1993) 1104.
[31] W. Huang, R. Sun, J. Tao, L.D. Menard, R. Nuzzo, J.M. Zuo, Nat. Mater. 7 (2008) 308–313.
[32] W.H. Qi, M.P. Wang, Y.C. Su, J. Mater. Sci. Lett. 21 (2002) 877–878.
[33] M. Dubiel, H. Hofmeister, E. Schurig, Phys. Status Solidi B 203 (1997) R5–R6.